Convergence studies for Enriched Free Mesh Method and its application to fracture mechanics

Hitoshi Matsubara[†] and Genki Yagawa[‡]

*Department of Civil Engineering and Architecture, University of the Ryukyus, 1, Senbaru,
Nishihara-cho, Okinawa 903-0213, Japan
Center for Computational Mechanics Research, Toyo University, 2-36-5,
Hakusan, Bunkyo-ku, Tokyo 112-0001, Japan*

Abstract. The Enriched Free Mesh Method (EFMM) is a patch-wise procedure in which both a displacement field on an element and a stress/strain field on a cluster of elements connected to a node can be defined. On the other hand, the Superconvergent Patch Recovery (SPR) is known to be an efficient post-processing procedure of the finite element method to estimate the error norm at a node. In this paper, we discuss the relationship between solutions of the EFMM and those of the SPR through several convergence studies. In addition, in order to solve the demerit of the smoothing effect on the fracture mechanics fields, we implement a singular stress field to a local patch in the EFMM, and its effectiveness is investigated.

Keywords: patch-wise mixed formulation; adaptive finite element method; enriched free mesh method; free mesh method; superconvergent patch recovery.

1. Introduction

With the finite element method (FEM), each process, such as defining geometrical shapes and physical fields, setting material properties and assigning boundary conditions, is done on an element-wise basis (Zienkiewicz and Taylor 2000), in which the meshing is the most important and time consuming process among others. For example, it is well known that the aspect ratio of an element plays the especially important role with respect to approximation accuracy. Therefore, we need robust mesh generation technologies that do not deteriorate this ratio (Giraud-Moreau *et al.* 2006).

One of the authors has proposed a numerical method (Yagawa and Yamada 1996, Yagawa and Furukawa 2000), which is called the Free Mesh Method (FMM), in which the mesh and the matrix of the system are generated in a node-by-node manner without the information for the mesh connectivity. Also, since the process of the FMM progresses with node by node, it is effective in

---

† E-mail: matsbara@tec.u-ryukyu.ac.jp
‡ Professor, Corresponding author, E-mail: yagawa@eng.toyo.ac.jp

parallel-computing technology (Fujisawa *et al*. 2003, Yagawa 2004). The FMM has been applied to various fields in the computational mechanics including complex and large-scale problems such as the aerodynamic sounds simulation of air-reed instrument (Tsuchida *et al*. 2006).

On the other hand, the adaptive-FEM is known to overcome the mesh dependency issues of the FEM by posteriori error estimations (Kelly *et al*. 1983a, 1983b), which can improve the geometrical state of elements with a large error norm. Since it is usually impossible to obtain an exact error norm, there have been several proposals for error estimation (Zhu 1997). Among these proposals, Zienkiewicz and Zhu (Zienkiewicz and Zhu 1992a, 1992b, 1992c) applied the localized lest squares method to the stresses in a local patch, which is known as the Superconvergent Patch Recovery (SPR), which results in highly accurate posteriori results. This least squares technique has been successfully applied to several numerical methods including the Element Free Galerkin method and so on (Belytschko *et al*. 1994, Liu *et al*. 1997).

Here, it is interesting to note that the FMM and the SPR share the following features:

(1) Based upon the FEM,

(2) Intends to resolve mesh dependency problems of the FEM,

(3) Calculates in node-wise manner, and

(4) Focuses the local patch around a node.

On the other hand, there are differences between these two methods, including:

(1) The SPR have been developed as a post-processing procedure though the FMM as a main-processing one, and

(2) The results of the SPR are more accurate than those of the FEM, though the results of the FMM are equal to those of the FEM.

As for improvement of the accuracy of the FMM, some attempts have been made (Kanto 2000, Matsubara *et al*. 2002, 2004, Yagawa and Miyamura 2005, Tian and Yagawa 2005, Tian *et al*. 2006a, Tian *et al*. 2006b). Among others, the element with the "generalized nodes" (Tian and Yagawa 2005) seems the most effective for accuracy improvements. The generalized nodes are formulated as an expansion of the generalized finite element method (GFEM) based on the Partition of Unity (Melenk and Babuska 1996), and the accuracy is equivalent to the quadratic finite elements with mid-side nodes (Tian and Yagawa 2005). Studied also is the Enriched Free Mesh Method (EFMM) (Yagawa and Matsubara 2007), which defines the displacement field on an element as well as the stress/strain field on a local patch, which is a cluster of elements connected to a node. In general, the elements with multiple fields are called mixed type elements, and have been developed to prevent the loss of accuracy due to the mesh distortion (Kasper and Taylor 2000a, 2000b). This kind of elements are known as the non-conforming element by Taylor *et al*. (Taylor *et al*. 1976) and then systematized by Simo *et al*. (Simo and Rifai 1990, Simo *et al*. 1992).

Considering that the EFMM is a methodology, which is modified using the idea of the SPR to the FMM, we study, in the present paper, the relationship between the EFMM and the SPR through several convergence studies. It is known that the numerical techniques based on the smoothing effects are not suitable for the problems with singular field. Thus, we study here the applicability of the EFMM to a problem of singular stress field.

In Chapters 2 and 3, the concepts of the FMM and the SPR are summarized, respectively. In Chapter 4, the EFMM is compared to the concept of the SPR. In Chapter 5, the accuracy and the convergence of the error norms are studied. In Chapter 6, we investigate the effectiveness of the EFMM for a linear fracture mechanics. We conclude the present study in Chapter 7.

2. Concept of Free Mesh Method (Yagawa and Yamada 1996)

The FMM requires only nodal information as its input data. The cluster of local elements called a local patch is automatically generated around a node called a central node. Fig. 1 shows how to generate a local patch and assemble a global stiffness matrix. On each node prepared in the domain beforehand, temporary local elements are first created by using the central node P_i, and its surrounding nodes S_1, S_2, ..., S_6 called as satellite nodes. On each temporary element, an element stiffness matrix is calculated in the next. Third, only the row components of the element matrix which relate to the central node are added to the pertinent row of the total stiffness matrix. After executing the above-mentioned processing with respect to other nodes, we can obtain the global stiffness matrix equal to that of the FEM.

The features of the FMM are summarized as follows:
(1) The local patch is generated around a node,
(2) The pre-processing in the conventional FEM is seamlessly connected with the main-processing, and
(3) The local elements are represented by the node-based data structure.

We note again that the FMM incorporates the mesh generation in main-processing though the conventional FEM requires the mesh generation in pre-processing. Consequently, the results obtained by the FMM are strictly equal to those of the FEM. Thus the FMM inherits the wealth of research results of the FEM that have been studied in the past.

3. Superconvergent Patch Recovery

The adaptive-FEM is known as a method that improves the accuracy of solutions by posteriori

(a) Domain of analysis

(b) Clustered local elements (local patch)
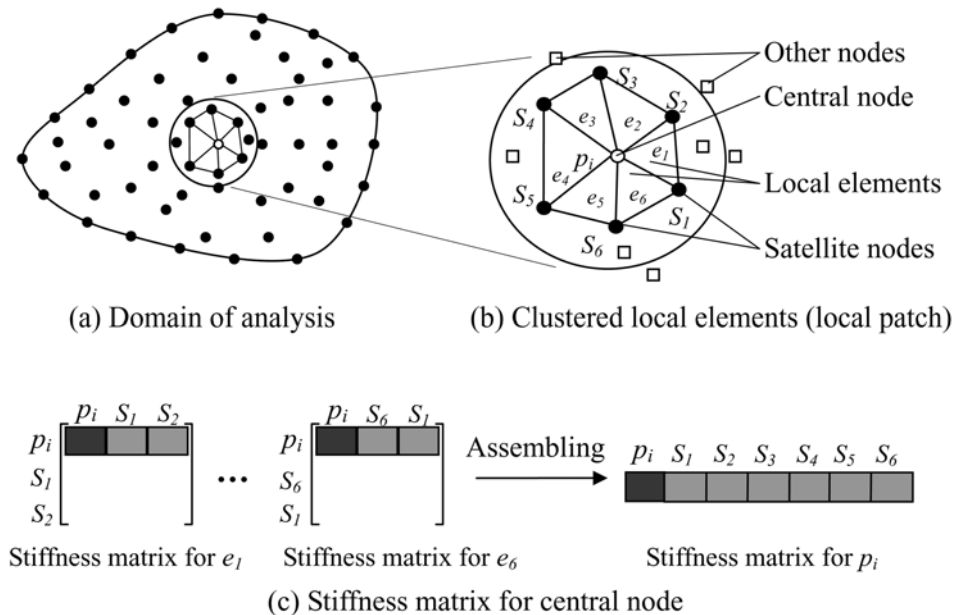
(c) Stiffness matrix for central node
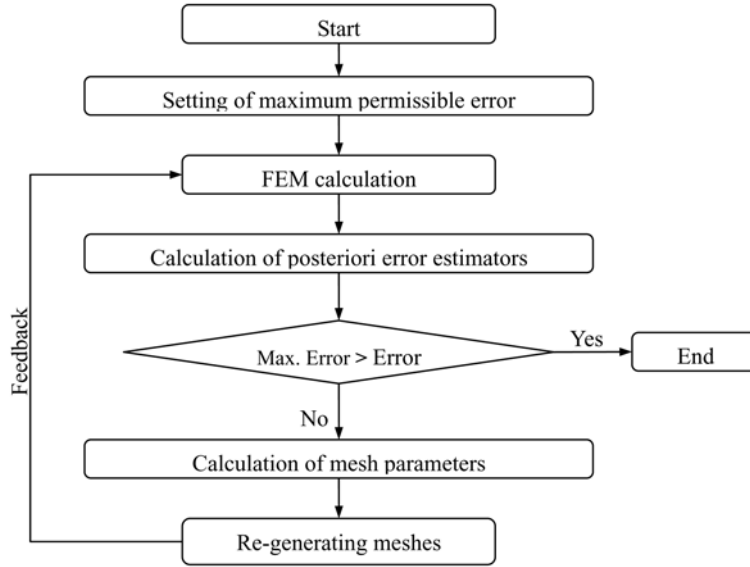
Fig. 1 Concept of Free Mesh Method

Fig. 2 Flowchart for adaptive finite element method

error estimations, updating the meshes into a more appropriate geometrical state. Fig. 2 shows the flowchart of the adaptive-FEM. To estimate the posteriori error, it is necessary to calculate the error norm, which is given as follows,

$$\mathbf{E} = \sqrt{\sum_{i=1}^{n} \left\| \sigma - \sigma^h \right\|_i^2} \tag{1}$$

where $\mathbf{E}$ is the error norm, n the number of sampling points in the local patch, σ^h the numerical result and σ the exact one. In usual, σ will be represented by the value, which is higher order approximation than that of the FEM.

Zienkiewicz and Zhu (Zienkiewicz and Zhu 1992a, 1992b, 1992c) studied the SPR to estimate the error norm of a node. As shown in Fig. 3, a higher order stress $\sigma*$ is obtained by applying the localized least squares method to the calculated stress on the local patch.

In the SPR, the $\sigma*$ is represented by using an arbitrary basis function as follows,

$$\sigma* \equiv P^T(\mathbf{x})\mathbf{a} \tag{2}$$

where $\mathbf{a}$ is an unknown parameter and $P^T(\mathbf{x})$ is an arbitrary function, which should have higher order functions than that of the elements. The relation between $\sigma*$ and σ^h is given by using the localized least squares method as follows,

$$\mathbf{Min}_{\mathbf{a}} \sum_{i=1}^{n} (\sigma*(\mathbf{x}_i) - \sigma^h(\mathbf{x}_i))^2 = \mathbf{Min}_{\mathbf{a}} \sum_{i=1}^{n} (P(\mathbf{x})^T \mathbf{a} - \sigma^h(\mathbf{x}_i))^2 \tag{3}$$

where n is the total number of sampling points and $\mathbf{x}_i$ is the coordinate of the sampling point as shown in Fig. 3. The stationary condition of Eq. (3) is

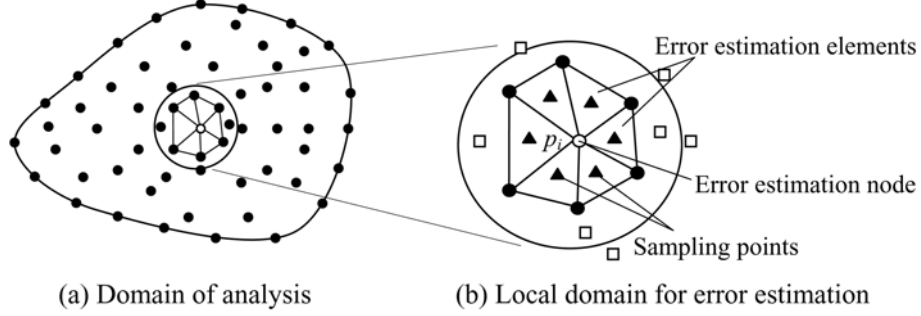(a) Domain of analysis   (b) Local domain for error estimation

Fig. 3 Concept of Superconvergent Patch Recovery

$$\sum_{i=1}^{n} [P^T(\mathbf{x}_i)P(\mathbf{x}_i)\mathbf{a} - P^T(\mathbf{x}_i)\boldsymbol{\sigma}^h(\mathbf{x}_i)] = 0 \qquad (4)$$

which yields

$$\mathbf{a} = \sum_{i=1}^{n} [(P^T(\mathbf{x}_i)P(\mathbf{x}_i))^{-1} P^T(\mathbf{x}_i)\boldsymbol{\sigma}^h(\mathbf{x}_i)] \qquad (5)$$

Substituting Eq. (5) into Eq. (2), we obtain

$$\boldsymbol{\sigma}^* \equiv P^T(\mathbf{x}) \sum_{i=1}^{n} [(P^T(\mathbf{x}_i)P(\mathbf{x}_i))^{-1} P^T(\mathbf{x}_i)\boldsymbol{\sigma}^h(\mathbf{x}_i)] \qquad (6)$$

In the SPR, the solutions of each element are smoothed on the local patch by using Eq. (6). Selecting an appropriate basis function and sampling points, we can obtain smoothed effective results. For example, it is known that assuming the finite element approximation with order of p, we can obtain the $\boldsymbol{\sigma}^*$ with order of p by using p-Gaussian points (Zienkiewicz and Zhu 1992c). It is note that the sampling points of more than the number of basis are necessary to calculate of a discrete system in Eq. (6) because the lack of those might lead $(P^T(\mathbf{x}_i)P(\mathbf{x}_i))^{-1}$ to a singular.

4. Enriched Free Mesh Method

4.1 Formulation of Enriched Free Mesh Method

As noted above, the SPR aims at the acquirement of a highly accurate result in post-processing, whereas the FMM aims at the establishment of a seamless procedure from the mesh generation to the calculation in main-processing. The basic idea of the EFMM is to integrate the FMM and the SPR, and to obtain a highly accurate result of the SPR in the main-processing (Yagawa and Matsubara 2007). The EFMM is one of the mixed finite element formulations (Zienkiewicz and Taylor 2000), in which the displacement field of each local element and the stress/strain field of a local patch are assumed independently (see Figs. 4(a) and 4(b)). The displacement field and the stress/strain field have been related by the least squares method or the Hellinger-Reissner principle (Yagawa and Matsubara 2007). Since all the processes in the EFMM progress with patch by patch,
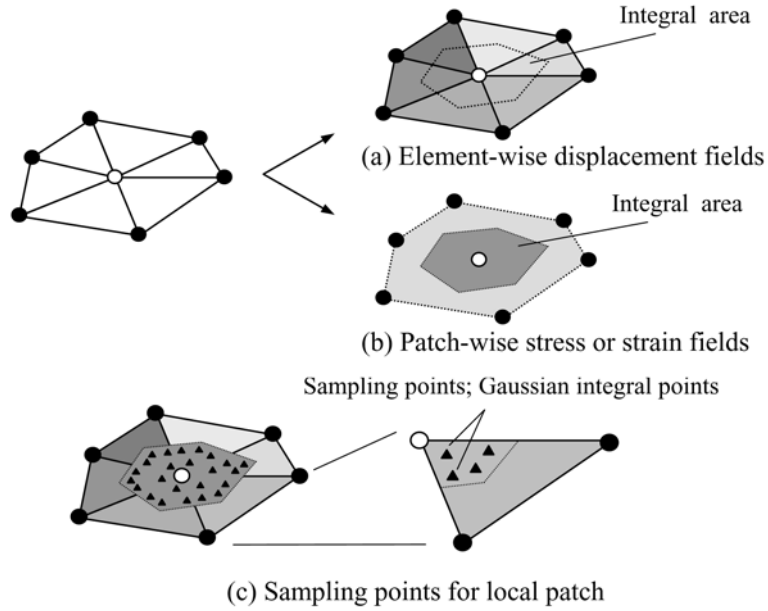
(a) Element-wise displacement fields

(b) Patch-wise stress or strain fields

(c) Sampling points for local patch

Fig. 4 Stress/strain enrichment on local patch

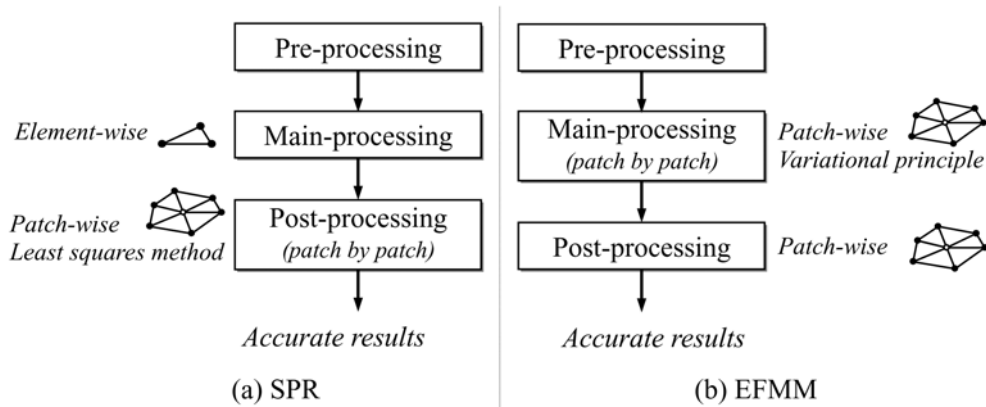(a) SPR   (b) EFMM

Fig. 5 Comparison between SPR and EFMM

the EFMM can be called a patch-wise procedure. Fig. 5 compares the procedure of the SPR versus that of the EFMM.

The Hu-Washizu principle, known as the generalized variational principle, allows us to define independent fields for stress, strain and displacement functions in a solid body (Zienkiewicz and Morgan 1983, Washizu 1968). With this principle, the formulation of the EFMM becomes more general compared to the least squares method or the Hellinger-Reissner principle (Yagawa and Matsubara 2007). Thus, we show the formulation of the EFMM based on the Hu-Washizu principle as follows,

Considering a linear elastic body, we can express the Hu-Washizu principle as

$$\Pi(\varepsilon, \sigma, \mathbf{u}) = \int_{\Omega} (\sigma(\mathbf{x}))^T \mathbf{B}\mathbf{d}d\Omega - \int_{\Omega} (\sigma(\mathbf{x}))^T \varepsilon(\mathbf{x})d\Omega + \frac{1}{2}\int_{\Omega} (\varepsilon(\mathbf{x}))^T \mathbf{D}\varepsilon(\mathbf{x})d\Omega - \int_{\Omega} (\mathbf{u}(\mathbf{x}))^T \tilde{\mathbf{b}}d\Omega - \int_{\Gamma} (\mathbf{u}(\mathbf{x}))^T \tilde{\mathbf{t}}d\Gamma \tag{7}$$

where Ω denotes the integral area in Fig. 4, $\tilde{\mathbf{b}}$ the body force and $\tilde{\mathbf{t}}$ the surface force on the boundary Γ (Zienkiewicz and Taylor 2000). We employ the Gaussian integral points as sampling points as shown in the figure. We require three or more Gaussian points in case of the 1st-order stress/strain field, meanwhile six or more points for 2nd-order case.

The displacement $\mathbf{u}(\mathbf{x})$ is interpolated as follows,

$$\mathbf{u}(\mathbf{x}) = {}^{u}\mathbf{N}\mathbf{d} \tag{8}$$

where $\mathbf{d}$ is the degrees of freedom and ${}^{u}\mathbf{N}$ the shape function. The strain-displacement matrix $\mathbf{B}$ is given by

$$\mathbf{B} = [\mathbf{b}_1 \ \mathbf{b}_2 \ \dots \ \mathbf{b}_n]$$

with (9)

$$\mathbf{b}_i = \begin{bmatrix} \partial^{u}\mathbf{N}_i / \partial x & 0 \\ 0 & \partial^{u}\mathbf{N}_i / \partial y \\ \partial^{u}\mathbf{N}_i / \partial y & \partial^{u}\mathbf{N}_i / \partial x \end{bmatrix}, \quad i = 1, 2, \dots, n$$

where n is the total degrees of freedom of a local element. In addition, the stress field $\sigma(\mathbf{x})$ and the strain field $\varepsilon(\mathbf{x})$ are, respectively, defined on a local patch by using the arbitrary basis function ${}^{\sigma}\mathbf{N}$ and ${}^{\varepsilon}\mathbf{N}$ as follows,

$$\varepsilon(\mathbf{x}) = {}^{\varepsilon}\mathbf{N}\mathbf{a} \tag{10}$$

and

$$\sigma(\mathbf{x}) = {}^{\sigma}\mathbf{N}\mathbf{b} \tag{11}$$

where $\mathbf{a}$ and $\mathbf{b}$ are the unknown coefficients, $\varepsilon(\mathbf{x})$ the $\{\varepsilon_{xx}, \varepsilon_{yy}, \gamma_{xy}\}^T$, $\sigma(\mathbf{x})$ the $\{\sigma_{xx}, \sigma_{yy}, \tau_{xy}\}^T$, ${}^{\varepsilon}\mathbf{N}$ an arbitrary basis function for strain and ${}^{\sigma}\mathbf{N}$ an arbitrary basis function for stress. Assuming the stress and strain fields without singularity, we can employ the following complete polynomial equation:

$$^{\varepsilon}\mathbf{N} = {}^{\sigma}\mathbf{N} = \begin{bmatrix} p^T(\mathbf{x}) & 0 & 0 \\ 0 & p^T(\mathbf{x}) & 0 \\ 0 & 0 & p^T(\mathbf{x}) \end{bmatrix} \tag{12}$$

where $p^T(\mathbf{x})$ is defined as follows,

$$\begin{aligned} p^T(\mathbf{x}) &= [1 \ x \ y] & linear-basis \\ p^T(\mathbf{x}) &= [1 \ x \ y \ xy \ x^2 \ x^2] & quadratic-basis \\ p^T(\mathbf{x}) &= [1 \ x \ y \ xy \ x^2 \ y^2 \ x^2y \ xy^2 \ x^3 \ y^3] \ cubic-basis \end{aligned} \tag{13}$$

In this paper, the EFMM with linear-basis and quadratic-basis stress/strain field is studied. The stationary conditions of Eq. (7) result in the following equations,

$$\int_\Omega \delta\varepsilon(\mathbf{x})^T (\mathbf{D}\varepsilon(\mathbf{x}) - \sigma(\mathbf{x})) d\Omega = 0 \tag{14}$$

$$\int_\Omega \delta\sigma(\mathbf{x})^T (\mathbf{Bd} - \varepsilon(\mathbf{x})) d\Omega = 0 \tag{15}$$

and

$$\int_\Omega \delta\mathbf{u}^T \mathbf{B}^T \sigma(\mathbf{x}) d\Omega - \int_\Omega \delta\mathbf{u}^T \tilde{\mathbf{b}} d\Omega - \int_\Gamma \delta\mathbf{u}^T \tilde{\mathbf{t}} d\Gamma = 0 \tag{16}$$

Thus, the matrix equation is given as follows,

$$\begin{bmatrix} \mathbf{A} & \mathbf{C} & \mathbf{0} \\ \mathbf{C}^T & \mathbf{0} & \mathbf{E} \\ \mathbf{0} & \mathbf{E}^T & \mathbf{0} \end{bmatrix} \begin{Bmatrix} \mathbf{a} \\ \mathbf{b} \\ \mathbf{d} \end{Bmatrix} = \begin{Bmatrix} \mathbf{0} \\ \mathbf{0} \\ \mathbf{f} \end{Bmatrix} \tag{17}$$

where

$$\mathbf{A} = \int_\Omega (^\varepsilon\mathbf{N})^T \mathbf{D}(^\varepsilon\mathbf{N}) d\Omega \tag{18}$$

$$\mathbf{C} = -\int_\Omega (^\varepsilon\mathbf{N})^T (^\sigma\mathbf{N}) d\Omega \tag{19}$$

$$\mathbf{E} = \int_\Omega {}^\sigma\mathbf{N}\mathbf{B} d\Omega \text{ and} \tag{20}$$

$$\mathbf{f} = \int_\Omega (^\mathrm{u}\mathbf{N})^T \tilde{\mathbf{b}} d\Omega + \int_\Gamma (^\mathrm{u}\mathbf{N})^T \tilde{\mathbf{t}} d\Gamma \tag{21}$$

By reducing the unknown coefficient $\mathbf{a}$ and $\mathbf{b}$ from Eq. (17) on a local patch, the following matrix equation is obtained:

$$\mathbf{k}_{\mathrm{HW}}\, \mathbf{d} = \mathbf{f} \tag{22}$$

where

$$\mathbf{k}_{\mathrm{HW}} = \mathbf{E}^T (\mathbf{C}^T\, \mathbf{A}^{-1}\, \mathbf{C})^{-1}\, \mathbf{E} \tag{23}$$

In the EFMM, this condensation is carried out in a patch by patch manner.

5. Convergence studies

5.1 Patch tests for constant stress and strain

A plane stress condition is considered for the patch tests of the EFMM (see Fig. 6), where the following displacement field is prescribed at the exterior nodes:
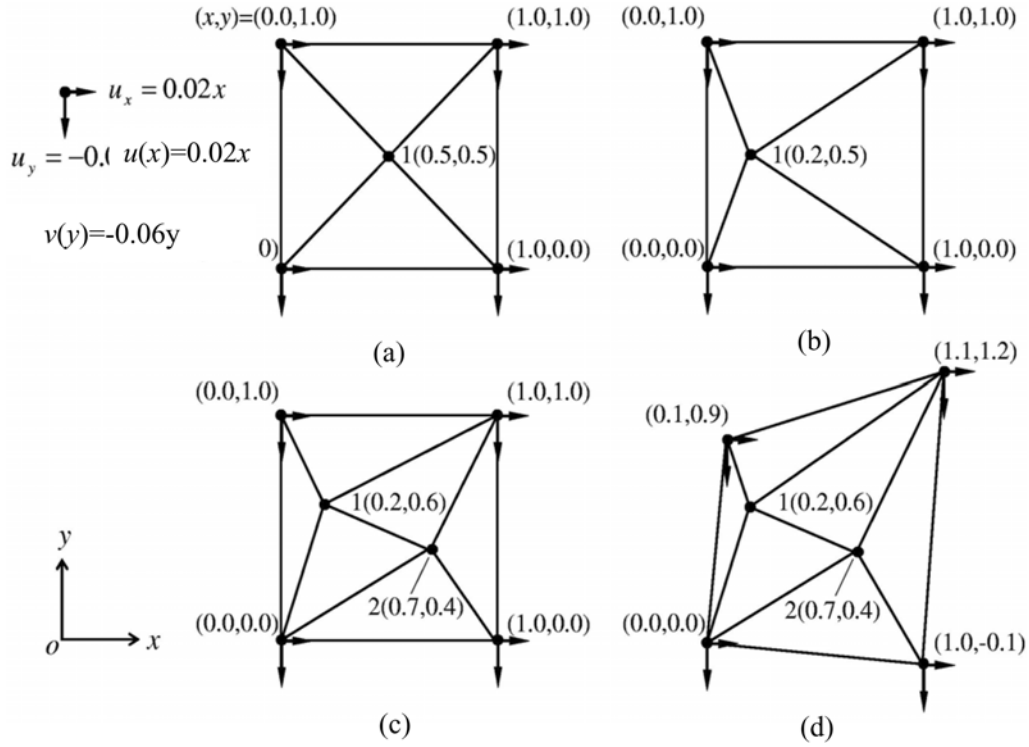
Fig. 6 Patch test of EFMM

Table 1 Result of patch test

Mesh	Node #	Coordinates		Displacement Numerical(Exact)	
		x	y	u	v
(a)	1	0.5	0.5	0.010(0.010)	-0.030(-0.030)
(b)	1	0.2	0.5	0.004(0.004)	-0.030(-0.030)
(c)	1	0.2	0.6	0.004(0.004)	-0.036(-0.036)
	2	0.7	0.4	0.014(0.014)	-0.024(-0.024)
(d)	1	0.2	0.6	0.004(0.004)	-0.036(-0.036)
	2	0.7	0.4	0.014(0.014)	-0.024(-0.024)

$$\left\{ \begin{matrix} u(x) \\ v(y) \end{matrix} \right\} = \left\{ \begin{matrix} 0.02x \\ -0.06y \end{matrix} \right\} \tag{24}$$

which results in $\varepsilon_{xx} = \partial u(x)/\partial x = 0.02$, $\varepsilon_{yy} = \partial v(y)/\partial y = -0.06$ and $\gamma_{xy} = \partial u(x)/\partial y + \partial v(y)/\partial x = 0$. Fig. 6(a) illustrates the regular mesh, Figs. 6(b) and (c) the irregular ones in a square plane, respectively, while Fig. 6(d) the irregular mesh in a non-square plane. As shown in Table 1, the patch tests pass regardless of the types of the meshes.
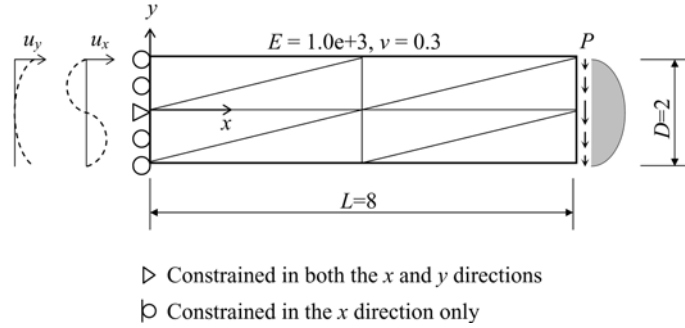
Fig. 7 Timoshenko's Cantilever beam under parabolic variation of applied shear traction P for error norm study

5.2 Convergence study of cantilever beam

In order to evaluate the convergence of the displacement and the energy, we take, respectively, the L_2 error norm in displacement, $\|E\|_u$, and the L_2 error norm in energy, $\|E\|_e$, as follows,

$$\|E\|_u = \sqrt{\int_\Omega (\mathbf{u} - \mathbf{u}^{exact})^T (\mathbf{u} - \mathbf{u}^{exact}) d\Omega} \quad \text{and} \tag{25}$$

$$\|E\|_e = \sqrt{\int_\Omega (\boldsymbol{\varepsilon} - \boldsymbol{\varepsilon}^{exact})^T (\boldsymbol{\sigma} - \boldsymbol{\sigma}^{exact}) d\Omega} \tag{26}$$

where $\mathbf{u}, \boldsymbol{\varepsilon}$ and $\boldsymbol{\sigma}$ are the numerical results of displacement, strain and stress, respectively, and $\mathbf{u}^{exact}, \boldsymbol{\varepsilon}^{exact}$ and $\boldsymbol{\sigma}^{exact}$ the exact values of the same, respectively. In the analysis, the bending problem of Timoshenko's cantilever beam (Timoshenko and Goodier 1970), whose length is 8, the height 2 and the width 1 as shown in Fig. 7, is employed. This model includes parabolic variation of applied shear traction at $x = L$ with essential boundary condition at $x=0$ to match the exact solution (Augarde and Deeks 2008). We assume a plane stress condition with the Poisson's ratio v of 0.3 and the Young's modulus $\mathbf{E}$ of 1.0e+3 as the material constants. Also, with the same pattern as the 2×2 mesh division shown in Fig. 7, we employ seven models of mesh divisions: 1×1, 2×2, 4×4, 8×8, 16×16, 32×32, and 64×64. In the examples, the 3-node constant strain element and the 6-node linear strain elements are, respectively, employed for the FEM. These FEM schemes are called as the FEM-T3 and the FEM-T6 in this paper, respectively. On the other hand, only the 3-node constant strain element is employed as the local element for the EFMM. The linear polynomial and the quadratic polynomial in Eq. (13) are, respectively, employed as the stress/strain field of a local patch in the EFMM. In this paper, these EFMM schemes are called as the EFMM-T3L and the EFMM-T3Q, respectively.

5.2.1 Comparison among FEM, SPR and EFMM

Fig. 8 shows the calculated results of the L_2 errors in energy versus number of nodes, where the 3-node constant strain elements are employed for all the cases. In the Figure, the SPR with 1st-order stress field and three Gaussian points are called SPR-T3. It is shown here that the accuracy level is better in the order of EFMM-T3Q, EFMM-T3L, SPR-T3 and FEM-T3. On the other hand, the convergence ratios R of these are, respectively, 1.8, 1.5, 1.5 and 1. Thus, it is concluded that the
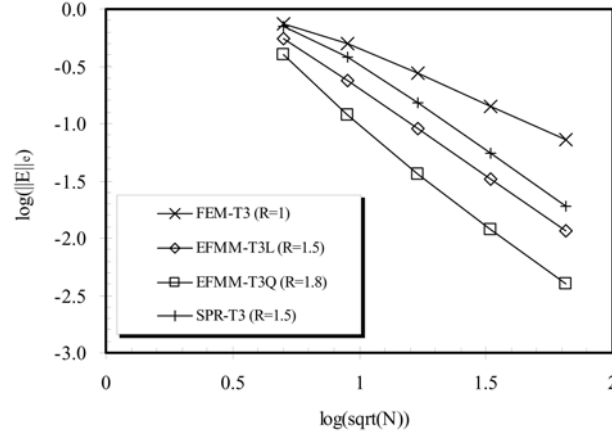
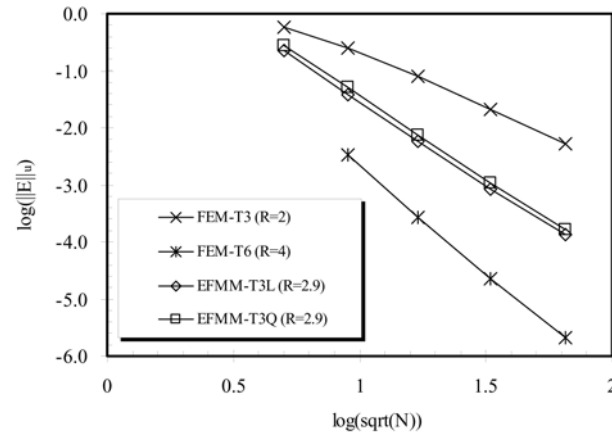Fig. 8 L_2 errors in energy: comparison between FEM, EFMM and SPR

Fig. 9 L_2 errors in displacements: comparison between linear and quadratic bases

results of the EFMMs outperform those of the FEM-T3 and the SPR-T3 in the accuracy and the convergence ratio.

5.2.2 Comparison between FEM and EFMM

Here, the accuracy of the EFMM is discussed by comparing the EFMM against the FEM. Figs. 9 and 10 show error norms in displacement and the energy, respectively, versus the number of nodes. We can conclude the followings with respect to the error norm in displacement (see Fig. 9):

(1) The results of the EFMM-T3L and the EFMM-T3Q are almost equivalent with respect to both the accuracy and the convergence.

(2) The accuracy of the EFMMs is between those of the FEM-T6 and the FEM-T3, and that of the FEM-T6 is the best.

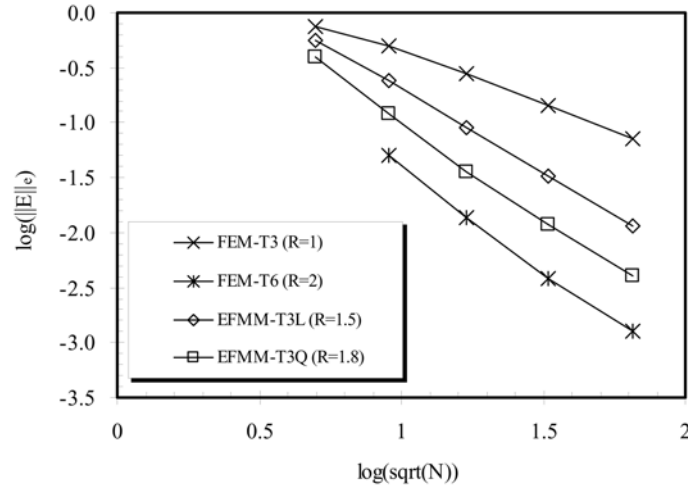(3) The convergence ratio of the EFMMs is nearly mean value of that of the FEM-T3 and that of the FEM-T6.

Fig. 10 L$_2$ errors in energy: comparison between linear and quadratic bases

On the other hand, we conclude the followings with respect to the error norm in energy (see Fig. 10):

(1) The best one and the worst one are again the FEM-T6 and FEM-T3, respectively. The result of the EFMM-T3Q and that of the EFMM-T3L are between those of the FEM-T6 and FEM-T3.
(2) The result of the EFMM-T3Q is rather better than that of the EFMM-T3L.

We note here that the EFMM with 3 nodes elements competes well with the FEM-T6 with 6 nodes elements.

6. Application of EFMM to fracture mechanics

Because the convergence of the EFMM-T3L is quite the same as the SPR (See Fig. 8), it can be said that the improvement of the accuracy by the EFMM is caused by the smoothing effect which is similar to the SPR. In general, it is considered that the numerical techniques based on the smoothing effects are not suitable for the problem with singular stress distributions because a large error might be involved with this singularity. Thus, in this chapter, we implement a singular stress field for the linear fracture mechanics to a local patch of the EFMM to study its effectiveness.

Analyzing crack problems accurately, we often use the singular stress and strain field in the numerical technique as in the case of the extended FEM (Moes *et al*. 1999). In the EFMM, an arbitrary stress/strain field can be assumed at the local patches independently of the displacement field at each element. Thus, we can define the singular stress field $\bar{\sigma}(\mathbf{x})$ as follows, in which the local coordinate system is employed as shown in Fig. 11,

$$\bar{\sigma}(\mathbf{x}) = {}^{\sigma}\overline{\mathbf{N}}\mathbf{K} \tag{27}$$

where $\mathbf{K} = \{K_I \; K_{II}\}^T$ is the set of the stress intensity factors. Assuming the stress field at the crack-tip to be ${}^{\sigma}\overline{\mathbf{N}}$, we can write as (Irwin 1957),
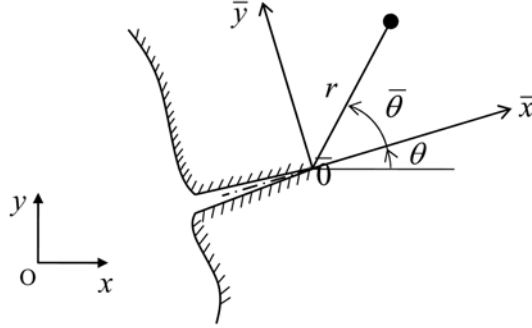
Fig. 11 Local coordinate system at a crack

$$
{}^{\sigma}\overline{\mathbf{N}} = \frac{1}{\sqrt{2\pi r}}
\begin{bmatrix}
\cos\dfrac{\overline{\theta}}{2}\left(1 - \sin\dfrac{\overline{\theta}}{2}\sin\dfrac{3\overline{\theta}}{2}\right) & -\sin\dfrac{\overline{\theta}}{2}\left(2 + \cos\dfrac{\overline{\theta}}{2}\cos\dfrac{3\overline{\theta}}{2}\right) \\[2ex]
\cos\dfrac{\overline{\theta}}{2}\left(1 + \sin\dfrac{\overline{\theta}}{2}\sin\dfrac{3\overline{\theta}}{2}\right) & \sin\dfrac{\overline{\theta}}{2}\cos\dfrac{\overline{\theta}}{2}\cos\dfrac{3\overline{\theta}}{2} \\[2ex]
\sin\dfrac{\overline{\theta}}{2}\cos\dfrac{\overline{\theta}}{2}\cos\dfrac{3\overline{\theta}}{2} & \cos\dfrac{\overline{\theta}}{2}\left(1 - \sin\dfrac{\overline{\theta}}{2}\sin\dfrac{3\overline{\theta}}{2}\right)
\end{bmatrix}
\tag{28}
$$

where the polar coordinates $(r, \overline{\theta})$, whose origin is at the crack-tip, is employed. In the global coordinate system of $x - y$, the stress field at the crack-tip can be expressed using the coordinate transform matrix $\mathbf{T}$ as follows,

$$
\sigma(\mathbf{x}) = \mathbf{T}^{-1}\overline{\sigma} = \mathbf{T}^{-1}({}^{\sigma}\overline{\mathbf{N}})\mathbf{K}
\tag{29}
$$

where $\mathbf{T}$ is defined as

$$
\mathbf{T} =
\begin{bmatrix}
\cos^2\theta & \sin^2\theta & 2\sin\theta\,\cos\theta \\
\sin^2\theta & \cos^2\theta & -2\sin\theta\,\cos\theta \\
-\sin\theta\,\cos\theta & \sin\theta\,\cos\theta & \cos^2\theta - \sin^2\theta
\end{bmatrix}
\tag{30}
$$

Assuming the elasticity problem, we can describe the relation between stress and strain as

$$
\sigma = \mathbf{D}\varepsilon
\tag{31}
$$

or

$$
\varepsilon = \mathbf{D}^{-1}\sigma
\tag{32}
$$

Then, we can eliminate the terms of strain unknowns in Eq. (10), resulting in the Hellinger-Reissner principle obtained on a local patch as follows,

$$
\Pi(\sigma, \mathbf{u}) = \frac{1}{2}\int_{\Omega}(\sigma(\mathbf{x}))^T\mathbf{D}^{-1}\sigma(\mathbf{x})d\Omega + \int_{\Omega}(\sigma(\mathbf{x}))^T\mathbf{B}\mathbf{u}\,d\Omega - \int_{\Omega}(\mathbf{u}(\mathbf{x}))^T\tilde{\mathbf{b}}\,d\Omega - \int_{\Gamma}(\mathbf{u}(\mathbf{x}))^T\tilde{\mathbf{t}}\,d\Gamma
\tag{33}
$$

The stationary conditions of Eq. (33) are given as

Crack tip node   Nodes neighboring from crack tip

Influence area   Extended influence area
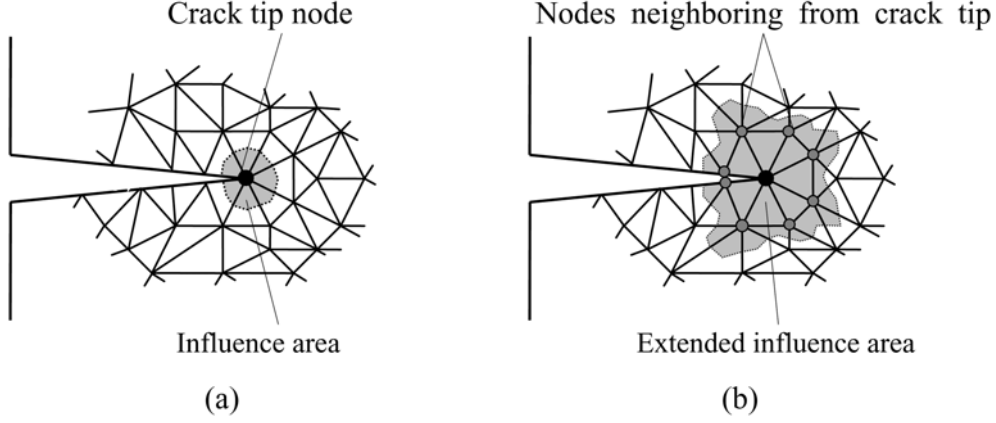
(a)   (b)

Fig. 12 Influence areas for singular stress of a crack tip

$$\int_{\Omega} \delta\boldsymbol{\sigma}(\mathbf{x})^T(\mathbf{B}\mathbf{d} - \mathbf{D}^{-1}\boldsymbol{\sigma}(\mathbf{x}))d\Omega = 0 \tag{34}$$

and

$$\int_{\Omega} \delta\mathbf{u}(\mathbf{x})^T\mathbf{B}^T\mathbf{D}^{\mathrm{u}}\mathbf{N}\mathbf{d}\,d\Omega - \int_{\Omega} \delta\mathbf{u}(\mathbf{x})^T\tilde{\mathbf{b}}\,d\Omega - \int_{\Gamma} \delta\mathbf{u}(\mathbf{x})^T\tilde{\mathbf{t}}\,d\Gamma = 0 \tag{35}$$

The matrix equation of the above equations is given as follows,

$$\begin{bmatrix} -\mathbf{A} & \mathbf{C} \\ \mathbf{C}^{\mathrm{T}} & \mathbf{0} \end{bmatrix}\begin{Bmatrix} \mathbf{K} \\ \mathbf{u} \end{Bmatrix} = \begin{Bmatrix} 0 \\ \mathbf{f} \end{Bmatrix} \tag{36}$$

where

$$\mathbf{A} = \int_{\Omega} (\mathbf{T}^{-1}(^{\sigma}\overline{\mathbf{N}}))^T\mathbf{D}^{-1}(\mathbf{T}^{-1}(^{\sigma}\overline{\mathbf{N}}))d\Omega \tag{37}$$

$$\mathbf{C} = \int_{\Omega} (\mathbf{T}^{-1}(^{\sigma}\overline{\mathbf{N}}))^T\mathbf{B}\,d\Omega \text{ and} \tag{38}$$

$$\mathbf{f} = \int_{\Omega} (^{\mathrm{u}}\overline{\mathbf{N}})^T\tilde{\mathbf{b}}\,d\Omega + \int_{\Gamma} (^{\mathrm{u}}\overline{\mathbf{N}})^T\tilde{\mathbf{t}}\,d\Gamma \tag{39}$$

Eq. (36) implies that the stress intensity factors, K_I and K_{II}, are directly obtained. Another advantage of the EFMM is that the formulation is carried out in exactly the same way as in the static elasticity problem that has been discussed in Chapter 4.

It is noted here that application of Eq. (36) to the crack-tip node only as shown in Fig. 12(a) is not enough to represent a stress singularity. In this paper, therefore, we applied Eq. (36) to both the crack-tip node and its satellite nodes (see Fig. 12(b)).

The analytical model and mesh are illustrated in Fig. 13 for the problem of a plate with a slanted center crack under uniform tension. The stress intensity factors, K_I and K_{II}, are obtained for various crack angles θ. We assume a plane stress condition with the Poisson's ratio ν of 0.32 and the Young's modulus $\mathbf{E}$ of 2.1e+6.
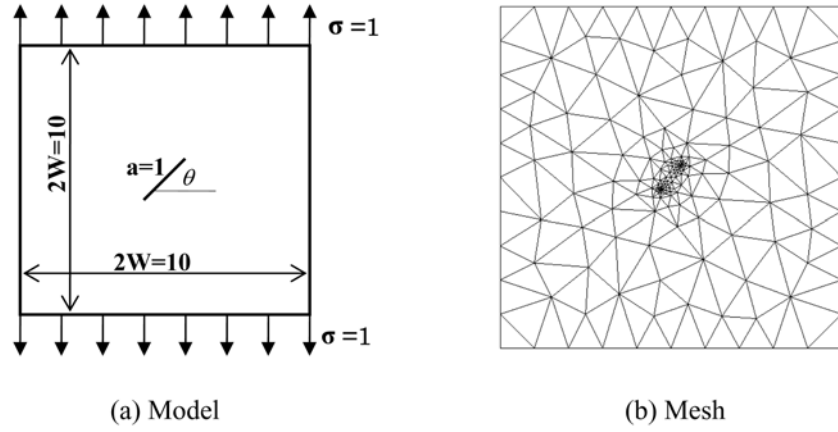
(a) Model   (b) Mesh

Fig. 13 Square plate with a slanted crack under uniform tension

(a) Distribution of KI
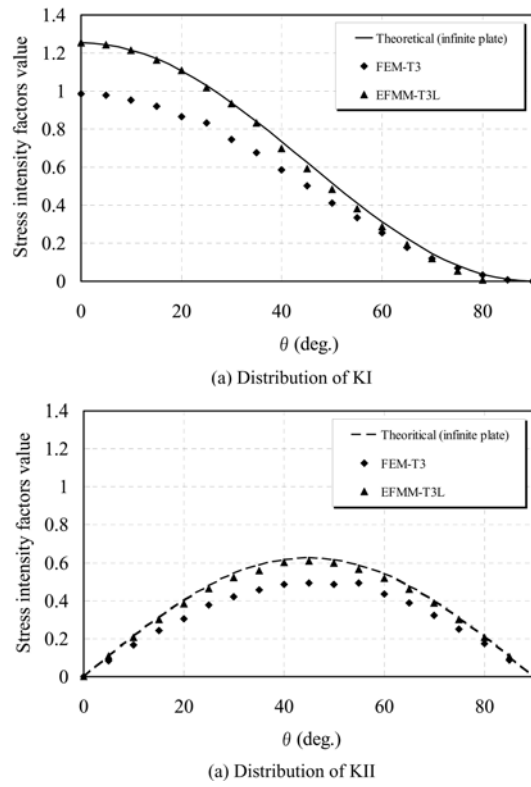

(a) Distribution of KII

Fig. 14 Comparison of stress intensity factors

Figs. 14(a) and (b) show the stress intensity factors, K_I and K_{II}, respectively, versus the angle of the crack. For the sake of comparison, the extrapolated stress intensity factors by the least-squares method based on the FEM-T3 are shown. From the figures, K_I and K_{II} values of the EFMM-T3L are much closer to the theoretical ones (Murakami 1987) than those of the FEM-T3. Therefore, it

can be said that the proposed technique solves the issue caused by the smoothing effects observed in singularity problem. In this numerical example, the stress singularity was considered on only the crack-tip node and the satellite nodes. However, we have not yet investigated the influence of the dimension of singular field, and here further work remains to be done.

7. Conclusions

In the present paper, we have studied the relationship among the FEM, the SPR and the EFMM through several convergence studies. As the result, it has been found that the EFMM is an effective method without additional nodes, showing reasonable accuracy behavior.

In order to solve the demerit of the smoothing effect for the singularity fields, we have successfully implemented a singular field to a local patch.

References

Augarde, C.E. and Deeks, A.J. (2008), "The use of Timoshenko's exact solution for a cantilever beam in adaptive analysis", *Finite. Elem. Anal. Des.*, **44**, 595-601.

Belytschko, T., Lu, Y.Y. and Gu, L. (1994), "Element-free Galerkin methods", *Int. J. Numer. Meth. Eng.*, **37**, 229-256.

Fujisawa, T., Inaba, M. and Yagawa, G. (2003), "Parallel computing of high-speed compressible flows using a node-based finite-element method", *Int. J. Numer. Meth. Eng.*, **58**, 481-511.

Giraud-Moreau, L., Borouchaki, H. and Cherouat, A. (2006), "A Remeshing Procedure for Numerical Simulation of Forming Processes in Three Dimensions", *Proceedings of the 15th International meshing roundtable*, Birmingham, September.

Irwin, G.R. (1957), "Analysis of stresses and stains near the end of a crack transverse a plate", *J. Appl. Mech.*, **24**, 361-364.

Kanto, Y. (2000), "Accurate Free Mesh Method by using Mixed Element", *Transaction of JSCES*, No. 20000036.

Kasper, E.P. and Taylor, R.L. (2000a), "A mixed-enhanced strain method - Part I: Geometrically linear problems", *Comput. Struct.*, **75**(3), 237-250.

Kasper, E.P. and Taylor, R.L. (2000b), "A mixed-enhanced strain method - Part II: Geometrically nonlinear problems", *Comput. Struct.*, **75**(3), 251-260.

Kelly, D.W., De, J.P., Gago, S.R., Zienkiewicz, O.C. and Babuska, I. (1983a), "A posteriori error analysis and adaptive processes in the finite element method: Part I - error analysis", *Int. J. Numer. Meth. Eng.*, **19**, 1593-1619.

Kelly, D.W., De, J.P., Gago, S.R., Zienkiewicz, O.C. and Babuska, I. (1983b), "A posteriori error analysis and adaptive processes in the finite element method: Part II - error analysis", *Int. J. Numer. Meth. Eng.*, **19**, 1621-1656.

Liu, W.K., Li, S. and Belytschko, T. (1997), "Moving Least Square Kernel Particle Method, Part 1: Methodology and Convergence", *Comput. Method. Appl. M.*, **143**, 113-154.

Matsubara, H., Iraha, S., Tomiyama, J. and Yagawa, G. (2002), "Application of 3D free mesh method to fracture analysis of concrete", *Proceedings of the 1st Asian Workshop on Meshfree Methods*, Singapore, December.

Matsubara, H., Iraha, S., Tomiyama, J., Yamashiro, T. and Yagawa, G. (2004), "Free mesh method using a tetrahedral element including vertex rotations", *Proceed. JSCE*, **766**(I-68), 97-107.

Melenk, J.M. and Babuska, I. (1996), "The partition of unity finite element method: Basic theory and applications", *Comput. Method. Appl. M.*, **139**, 289-314.

Moes, N., Dolbow, J. and Belytschko, T. (1999), "A finite element method for crack growth without remeshing",

Int. J. Numer. Meth. Eng., **46**, 131-150.

Murakami, Y. (1987), *Stress Intensity Factors Handbook*, Pergamon, New York, NY.

Simo, J.C. and Rifai, M.S. (1990), "A class of mixed assumed strain methods and the method of incompatible modes", *Int. J. Numer. Meth. Eng.*, **29**, 1595-1638.

Simo, J.C., Srmero, F. and Taylor, R.L. (1992), "Geometrically nonlinear enhanced strain mixed methods and the method of incompatible modes", *Int. J. Numer. Meth. Eng.*, **33**, 1413-1449.

Taylor, R.L., Beresford, P.J. and Wilson, E.L. (1976), "A non-conforming element for stress analysis", *Int. J. Numer. Meth. Eng.*, **10**, 1211-1219.

Tian, R. and Yagawa, G. (2005), "Generalized nodes and high-performance elements", *Int. J. Numer. Meth. Eng.*, **64**, 2039-2071.

Tian, R., Matsubara, H. and Yagawa, G. (2006a), "Linear dependence problems of partition of unity-based generalized FEMs", *Comput. Method. Appl. M.*, **195**, 4768-4782.

Tian, R., Matsubara, H. and Yagawa, G. (2006b), "Advanced 4-node tetrahedrons", *Int. J. Numer. Meth. Eng.*, **68**(12), 1209-1231.

Timoshenko, S.P. and Goodier, J.N. (1970), *Theory of Elasticity*, McGraw-Hill, Columbus, OH.

Tsuchida, J., Fujisawa, T. and Yagawa, G. (2006), "Direct numerical simulation of aerodynamic sounds by a compressible CFD scheme with node-by-node finite elements", *Comput. Method. Appl. M.*, **195**, 1996-1910.

Washizu, K. (1968), *Variational Methods in Elasticity and Plasticity*, Pergamon Press, New York, NY.

Yagawa, G. and Yamada, T. (1996), "Free Mesh Method: A New Meshless Finite Element Method", *Comput. Mech.*, **18**, 383-386.

Yagawa, G. and Furukawa, T. (2000), "Recent Developments of Free Mesh Method", *Int. J. Numer. Meth. Eng.*, **47**, 1419-1443.

Yagawa, G. (2004), "Node-by-Node Parallel Finite Elements: A Virtually Meshless Method", *Int. J. Numer. Meth. Eng.*, **60**, 69-102.

Yagawa, G. and Miyamura, T. (2005), "Three-node Triangular Shell Element Using Mixed Formulation and Its Implementation by Free Mesh Method", *Comput. Struct.*, **83**, 2066-2076.

Yagawa, G. and Matsubara, H. (2007), "Enriched Free Mesh Method: An accuracy improvement for Node-based FEM", *Comput. Plasticity*, **7**, 207-209.

Zhu, J.Z. (1997), "A posteriori error estimation-the relationship between different procedures", *Comput. Method. Appl. M.*, **150**, 411-422.

Zienkiewicz, O.C. and Morgan, K. (1983), *Finite element and approximation*, John Wiley & Sons.

Zienkiewicz, O.C. and Zhu, J.Z. (1992a), "The superconvergent patch recovery and a posteriori error estimates. PART1: The recovery technique", *Int. J. Numer. Meth. Eng.*, **33**, 1331-1364.

Zienkiewicz, O.C. and Zhu, J.Z. (1992b), "The superconvergent patch recovery and a posteriori error estimates. PART2: Error estimates and adaptivity", *Int. J. Numer. Meth. Eng.*, **33**, 1365-1382.

Zienkiewicz, O.C. and Zhu, J.Z. (1992c), "The superconvergent patch recovery (SPR) and adaptive finite element refinement", *Comput. Method. Appl. M.*, **101**, 207-224.

Zienkiewicz, O.C. and Taylor, R.L. (2000), *The finite element method*, fifth edition, Butterworth Heinemann.